Iranian Journal of Numerical Analysis and Optimization
Vol. 15, No. 1, 2025, pp 124–162
https://doi.org/10.22067/ijnao.2024.88668.1463
https://ijnao.um.ac.ir/

Research Article

Effect of demographic stochasticity in the persistence zone of a two-patch model with nonlinear harvesting

D. Mondal, M. Sen* and P.S. Mandal

Abstract

In this study, Allee type, single-species (prey), two-patch model with nonlinear harvesting rate, and species migration across two patches have been developed and analyzed. As we all know, the population of any species in an ecosystem is greatly dependent on the carrying capacity of the corresponding ecosystem; the main focus of our work is on how carrying capacity affects system dynamics in the presence and absence of randomness (deterministic and stochastic case, respectively). In the deterministic case,

*Corresponding author

Received 25 June 2024; revised 24 August 2024; accepted 16 September 2024

Debjani Mondal
Department of Mathematics, National Institute of Technology Patna, Patna, Bihar, India. e-mail: debjanim.phd20.ma@nitp.ac.in

Moitri Sen
Department of Mathematics, National Institute of Technology Patna, Patna, Bihar, India. e-mail: moitri300784@gmail.com

Partha Sarathi Mandal
Department of Mathematics, National Institute of Technology Patna, Patna, Bihar, India. e-mail: parthas@nitp.ac.in

How to cite this article
Mondal, D. Sen, M. and Mandal, P.S., Effect of demographic stochasticity in the persistence zone of a two-patch model with nonlinear harvesting. *Iran. J. Numer. Anal. Optim.*, 2025; 15(1): 124-162. https://doi.org/10.22067/ijnao.2024.88668.1463

we find that the carrying capacity of both patches increases the number of interior equilibrium points, and a maximum of eight interior equilibrium points can be observed. Also, we observe some interesting dynamics, including bi-stability, tri-stability, and catastrophic bifurcations. On the other hand, we use the continuous-time Markov chain modeling approach to construct an equivalent stochastic model of the corresponding deterministic model based on deterministic assumptions. Based on the extinction or persistence of the species, we compare the dynamics of deterministic and stochastic models in order to assess the impact of demographic stochasticity on the population of the species in two patches. The stochastic model shows the possibility of species extinction in a finite amount of time, whereas the deterministic model shows the persistence of the species at the same time, which is the major difference between these two models. We also derive the implicit equation for the expected time needed for species extinction. Finally, a graphic is used to illustrate how the patch's carrying capacity affects the expected time.

AMS subject classifications (2020): Primary 60J27; Secondary 34C23, 92-10.

Keywords: Stability analysis; Bifurcation; Continuous-time Markov chain (CTMC); Expected time to extinction.

1 Introduction

Every ecosystem is affected by biotic exploitation, habitat fragmentation, nutrient loading, and slow changes in the climate [29]. Normally, it is believed that nature would adapt to changes in the environment smoothly and continuously. Ecosystems' external factors, such as temperature, fertilizer or hazardous chemical inputs, groundwater depletion, habitat fragmentation, harvesting, or loss of species diversity, may vary over time gradually, even linearly. Additionally, nature is significantly impacted at both the local and global levels by the interplay between human activities and the ecosystem. The survival of several rare and endangered species may be hampered by the indiscriminate collection of biological resources. Therefore, in order to get the greatest advantages while maintaining ecological balance, harvesting should be done very judiciously. A population in the ecosystem may

abruptly switch from one stable state to another as a result of irresponsible harvesting; such a scenario is referred to as a regime shift or catastrophic alteration [7, 30, 29]. If a regime shift has taken place, it will be impossible to recover the population level to its prior state. As a result, the individuals of the specific population should continue to perform at their current low level of productivity [25]. The term "shift" describes minor frequency and large-scale variations in ecosystems that are likely to result in changes to the ecological framework, species abundances, and community organization [25, 27]. In such cases, both exploited and unexploited populations' abundances change throughout time. When an alternate stable equilibrium arises in an ecosystem, multiple stable equilibria exist in the fundamental deterministic structure, and a variety of fascinating things can take place. Furthermore, we can see that the ecosystem contains two alternate stable states under certain environmental circumstances, which are separated by an unstable equilibrium that delineates the boundary between the "basins of attraction" of the states.

Basically, the Allee effect is a phenomenon in ecology where the fitness (survival and reproduction) of individuals in a community rises with growing population size, especially at low population densities. In a deterministic setting, the Allee effect reveals population bi-stability [11]. However, in the case of the density-regulated growth process, it is possible that there might be more than one stable state in the presence of harvesting. Single-species models with and without the Allee effect and density-regulated parameter (θ) have been taken into consideration by several researchers [32, 26, 6, 28, 27]. Depending on the value of θ, the per capita growth rate (PGR) profile of the species is convex (when $\theta > 1$) or concave (when $\theta < 1$) in nature. It should be noted that when $\theta = 1$, the theta-logistic model becomes the classical logistic model. In major cases, the correlations between density and PGR among various species are concave in nature. The density-dependent theta logistic model can provide an explicit explanation of this type of relationship [32, 26]. The theta-logistic model with harvesting in Allee-type phenomena describes how population's growth is influenced by factors like intra-specific competition (described by the parameter θ), Allee effects (which cause population

growth to decrease at low population densities), and harvesting (removing individuals from the population).

According to the theory of patch dynamics, which is used in ecology, it is possible to understand an ecosystem's dynamics by examining its smaller, interconnected spatial components, which interact with one another, and this dynamics refers to the changes that take place in distinct geographic components of an ecosystem. The idea of patch dynamics is founded on the observation that ecosystems are spatially heterogeneous, meaning they include a variety of creatures and resources that are dispersed unevenly, and this heterogeneity occurs across scales of time and space. As we know, the number of individuals in any patch depends on the carrying capacity of the corresponding patch; therefore, our main aim is to study the effect of the patch's carrying capacity on the system dynamics.

Researchers might convert the simple theta-logistic model with harvesting into a two-patch system for several reasons: realism, migration and connectivity, habitat quality, metapopulation dynamics, management, and conservation. All the above-mentioned situations motivate us to consider the theta-logistic model with nonlinear harvesting in the Allee phenomena, which are distributed over two patches. On the other hand, a two-patch system refers to a more complex model that involves two interconnected subpopulations or habitats. In each patch, different ecological processes can occur, such as birth, death, migration between patches, and environmental interactions.

In [32, 26, 6, 28, 27], researchers studied the theta-logistic model for single species from different angles (deterministic and stochastic). A stochastic model can be utilized to study the volatility and variability present in biological systems as a result of demography or climate when a small number of individuals are present in a population [20, 13, 18]. In a stochastic model, there is a possibility of species extinction when a small number of individuals are initially present in the population. Sau, Bhattacharya, and Saha [27] considered two deterministic models: One is a density regulation model, and the other is an Allee-type density regulation model. Also, they considered both linear and nonlinear harvesting rates. For both models, they formulated and analyzed an equivalent stochastic differential equation (SDE) model by introducing demographic noise. Sibly et al. [32] investigated the

effect of density regulation around carrying capacity (θ in the theta-logistic model) on the correlation between the PGR and the population density. The authors of [26] established a deterministic model for a population that is subject to a strong Allee effect and conducted a model-based investigation on a population of economically significant herring fish. By taking demographic noise into account, they formulated an equivalent SDE model and calculated the probability of population extinction and the expected time to extinction. Bhowmick et al. [6] developed analogous SDE models of logistic and extended logistic growth models to examine the numerous real-life population dynamics and share the primary body of literature on stochastic modeling of ecological systems. For the mean, variance, and skewness of the quasi-equilibrium distribution under a more general family of growth curves, they developed a number of new approximations. Sau, Saha, and Bhattacharya [28] established a theta-logistic model by incorporating an Allee effect, crowding effects that lower birth and death rates in large populations, and two harvesting model options: linear harvesting and nonlinear harvesting. They constructed and analyzed the equivalent SDE models for their suggested models by including demographic stochasticity.

Several researchers utilized the continuous-time Markov chain (CTMC) modeling approach to construct and analyze stochastic models in the fields of epidemiology and ecology [1, 12, 13, 14, 17, 20, 22, 16, 15, 23, 21, 33, 34]. Akhi et al. [1] looked at a deterministic vector-host malaria model and changed it into a stochastic model using a CTMC and an SDE. They investigated how the model parameters affected the model outcomes by employing the Latin hypercube sampling and partial rank correlation coefficients procedure. Maity and Mandal [13] investigated the impact of demographic stochasticity on the transmission dynamics of cassava disease. Using the multi-type GWbp, they estimated the disease extinction probability for the stochastic model. The authors in [20] created a stochastic honeybee-virus model and estimated disease extinction probability using multi-type GWbp. They also examined how model parameters affected model results. An equivalent stochastic model of the deterministic Zika virus transmission model was created by the authors in [14]. They calculated the probability of disease extinction using the multi-type GWbp. After deriving an implicit equation

for the mean initial passage time, they looked at how the model's parameters affected the same. Maliyoni [15] developed a stochastic epidemic model based on the assumptions of the deterministic model for the West Nile virus in birds, and he concluded that the probability of disease extinction would be high when the disease spreads from exposed mosquitoes rather than infected birds and infected mosquitoes. Nipa, Jang, and Allen [23] developed two stochastic epidemic models for dengue fever, namely the CTMC model and the SDE model, based on the assumptions of the deterministic model. The stochastic models are nonhomogeneous in time because of the vector population's periodicity. They calculated the probability of disease extinction in close proximity to the disease-free periodic solution. Stephano et al. [33] studied the transmission dynamics of bovine tuberculosis in humans and cattle by considering both deterministic and CTMC models. They compared the probability of disease extinction estimated by the multi-type GWbp with the probability calculated by the CTMC model's sample paths. Swift [34] formulated and analyzed a stochastic prey-predator model, but in this investigation, they ignored the impact of demographic stochasticity on the extinction or persistence of the species in the population. The predator-prey model with parasites, in which prey individuals serve as the intermediate hosts for the parasites, was researched by Jang and Baglama [12]. They came to the conclusion that species in the population always become extinct when demographic stochasticity is present, but they remain in the population when stochasticity is not present. Indeed the authors did not study the mean time of species extinction in their investigation. In addition, the researchers in [32, 26, 6, 28, 27] did not use the CTMC modeling approach to develop and assess an analogous stochastic model of the theta logistic model. To the best of our knowledge, no one has yet used the CTMC modeling method to explore the stochastic version of a single-species, two-patch model with a nonlinear harvesting rate and species migration between two patches. Keeping in mind that, we will look into the following points:

(i) To understand how fluctuations in carrying capacity might alter the dynamics of the system.

(ii) To formulate an equivalent stochastic model of our suggested deterministic model by employing the CTMC modeling approach.

(iii) Compare deterministic and stochastic models based on species extinction and persistence.

(iv) Derive the implicit equation for the meantime to population extinction.

(v) A graphical illustration of how the patch's carrying capacity affects the possibility of population extinction and the mean time to extinction.

The organization of the remaining part of our article is as follows: In Section 2, we present our proposed deterministic model. By employing phase plane analysis, we examine the existence and stability of the equilibrium points of the model in subsection 3.1. In subsection 3.2, we conduct one-parametric and two-parametric bifurcation analysis to investigate how the carrying capacity of the patch affects the dynamics of the system. By using the CTMC modeling approach, we develop an identical stochastic model based on the assumptions of our proposed model in Section 4. A comparison of deterministic and stochastic models based on species extinction or persistence is given in subsection 4.1. We derive an implicit equation to compute the expected time to population extinction in subsection 4.2, and the graphical demonstration of the effect of the patch's carrying capacity on this time is provided in subsection 4.2.1. Finally, in Section 5, we provide a summary of our findings and their corresponding significance.

2 Deterministic model

First of all, we propose an Allee type density-regulated, single-species, two-patch model with nonlinear harvesting rate, and species migration across two patches. The base model is taken from [28, 27]. The mathematical representation of our proposed model is given by the following system of nonlinear equations:

$$\frac{dX_1}{dt} = r_1 X_1 \left(\frac{X_1}{K_1} - \frac{A_1}{K_1}\right)\left(1 - \left(\frac{X_1}{K_1}\right)^{\theta}\right) - \frac{q_1 E_1 X_1}{b_1 E_1 + L_1 X_1} + \beta_{21} X_2 - \beta_{12} X_1, \tag{1a}$$

$$\frac{dX_2}{dt} = r_2 X_2 \left(\frac{X_2}{K_2} - \frac{A_2}{K_2}\right)\left(1 - \left(\frac{X_2}{K_2}\right)^{\theta}\right) - \frac{q_2 E_2 X_2}{b_2 E_2 + L_2 X_2} + \beta_{12} X_1 - \beta_{21} X_2, \tag{1b}$$

with initial conditions $X_1(0) \geq 0$ and $X_2(0) \geq 0$. Here $X_i(t)$ represents the density of the prey population at time t in patch i, $i = 1, 2$. Species X_i has an intrinsic growth rate, denoted by the constant r_i. Moreover, K_i and A_i denote the carrying capacity and the Allee threshold of patch i, respectively, satisfying the condition $0 < |A_i| < K_i$, and θ is the density regulation around carrying capacity. Also, q_i and E_i represent the catchability coefficient and the harvesting effort in region i, respectively. The rates at which species move from patch 1 to patch 2 and from patch 2 to patch 1 are represented by the parameters β_{12} and β_{21}, respectively. Finally, b_i represents the degree of competition among the boats, fishermen, and other technology used in fishing in patch i. In patch i, L_i is the product of capture rate and handling time.

In our analysis, we put $\theta = 1$ in the system (1), and as a result, our modified system is as follows:

$$\frac{dX_1}{dt} = r_1 X_1 \left(\frac{X_1}{K_1} - \frac{A_1}{K_1}\right)\left(1 - \frac{X_1}{K_1}\right) - \frac{q_1 E_1 X_1}{b_1 E_1 + L_1 X_1} + \beta_{21} X_2 - \beta_{12} X_1, \tag{2a}$$

$$\frac{dX_2}{dt} = r_2 X_2 \left(\frac{X_2}{K_2} - \frac{A_2}{K_2}\right)\left(1 - \frac{X_2}{K_2}\right) - \frac{q_2 E_2 X_2}{b_2 E_2 + L_2 X_2} + \beta_{12} X_1 - \beta_{21} X_2. \tag{2b}$$

Figure 1 provides an illustration of the dynamics of the system (2).

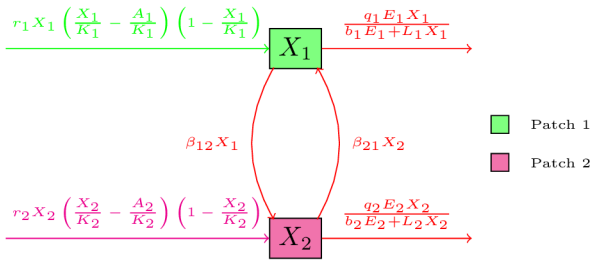

Figure 1: Compartmental diagram for the two-patch model (2).

3 Model analysis

The system (2) can be written as

$$\frac{dX_1}{dt} = F_1(X_1, X_2) \equiv \beta_{21} X_2 - \beta_{12} p_1(X_1), \tag{3a}$$

$$\frac{dX_2}{dt} = F_2(X_1, X_2) \equiv \beta_{12} X_1 - \beta_{21} p_2(X_2), \tag{3b}$$

where

$$p_1(X_1) = X_1 + \frac{q_1 E_1}{\beta_{12}(b_1 E_1 + L_1 X_1)} X_1 - \frac{r_1}{\beta_{12}} X_1 \left(\frac{X_1}{K_1} - \frac{A_1}{K_1}\right)\left(1 - \frac{X_1}{K_1}\right),$$

$$p_2(X_2) = X_2 + \frac{q_2 E_2}{\beta_{21}(b_2 E_2 + L_2 X_2)} X_2 - \frac{r_2}{\beta_{21}} X_2 \left(\frac{X_2}{K_2} - \frac{A_2}{K_2}\right)\left(1 - \frac{X_2}{K_2}\right).$$

It is important to note that as per the Picard's theorem, the above initial value problem (3) exhibits unique solution corresponding to any initial condition $X_1(0) \geq 0, X_2(0) \geq 0$, which is positively invariant [10].

The Jacobian matrix for the system (3) at any point $E_i^* = (X_1, X_2)$ is

$$J_{E_i^*} = \begin{bmatrix} -\beta_{12} p_1'(X_1) & \beta_{21} \\ \beta_{12} & -\beta_{21} p_2'(X_2) \end{bmatrix}.$$

Hence, for the stability of an equilibrium point, say (X_1^*, X_2^*), we need the following two conditions to be satisfied:

$$\beta_{12} p_1'(X_1^*) + \beta_{21} p_2'(X_2^*) > 0, \tag{4a}$$

$$p_1'(X_1^*) p_2'(X_2^*) > 1. \tag{4b}$$

3.1 Phase-plane analysis

In this section, we focus on examining the existence of equilibrium points. The system has only one trivial equilibrium point $(0, 0)$, and no other axial equilibrium points exist. Ecologically feasible interior equilibrium points are the point of intersection of the nullclines of prey in patch 1, $F_1(X_1, X_2) \equiv \beta_{21} X_2 - \beta_{12} p_1(X_1)$ and the nullclines of prey in patch 2, $F_2(X_1, X_2) \equiv \beta_{12} X_1 - \beta_{21} p_2(X_2)$. The interior equilibrium points are repre-

sented by the symbol $E_i^*(X_1^*, X_2^*)$. To get the number of interior equilibrium points, it is extremely complicated to analytically solve the two equations provided above, but the possible number of feasible interior equilibrium points in the system (2) can be determined from the relative positions and shapes of the nontrivial nullclines as shown in Figures 2 and 3(a). These figures are the graphical representation of the two nontrivial nullclines, which can intersect at a maximum of eight points. Therefore, we have observed that the system (2) has at most eight interior equilibrium points, and they may vary from zero to eight, namely, $E_i^*(X_1^*, X_2^*)$, $i = 1, \ldots, 8$, which is presented in Figure 2. We can confirm the stability characteristics of these nine equilibria by using the geometrical criteria given in (4) and the direction of the vector field (see Figure 3(c)), which are presented in the following propositions.

Proposition 1. The point $E_0(0, 0)$ is always locally asymptotically stable equilibrium point.

Proof. We have $F_1(X_1, X_2) = \beta_{21}X_2 - \beta_{12}p_1(X_1)$ and $F_2(X_1, X_2) = \beta_{12}X_1 - \beta_{21}p_2(X_2)$. Then the Jacobian matrix at E_0 is

$$J_{E_0^*} = \begin{bmatrix} -\beta_{12}p_1'(0) & \beta_{21} \\ \beta_{12} & -\beta_{21}p_2'(0) \end{bmatrix},$$

where $p_1'(X_1)|_{(0,0)} = 1 + \frac{q_1}{\beta_{12}b_1} + \frac{r_1A_1}{\beta_{12}K_1}$ and $p_2'(X_2)|_{(0,0)} = 1 + \frac{q_2}{\beta_{21}b_2} + \frac{r_2A_2}{\beta_{21}K_2}$.

Then we see that, the stability conditions (4), $\beta_{12}p_1'(0) + \beta_{21}p_2'(0) > 0$ and $p_1'(0)p_2'(0) > 1$ are satisfied at (0,0). Therefore, $E_0(0, 0)$ is always locally asymptotically stable. □

Proposition 2. (a) E_1^*, E_3^*, E_6^*, and E_7^* are always saddle points, if exist.
(b) E_2^*, E_4^*, and E_8^* are always locally asymptotically stable points, if exist.
(c) E_5^* is always unstable node, if exists.

Proof. The Jacobian matrix of the system (2) at any equilibrium point $E_i^*(X_1^*, X_2^*)$, $i = 1, 2, 3, 4, 5, 6, 7, 8$ can be written as,

$$J_{E_i^*} = \begin{bmatrix} \frac{\partial F_1}{\partial X_1} & \frac{\partial F_1}{\partial X_2} \\ \\ \frac{\partial F_2}{\partial X_1} & \frac{\partial F_2}{\partial X_2} \end{bmatrix}_{E_i^*}.$$

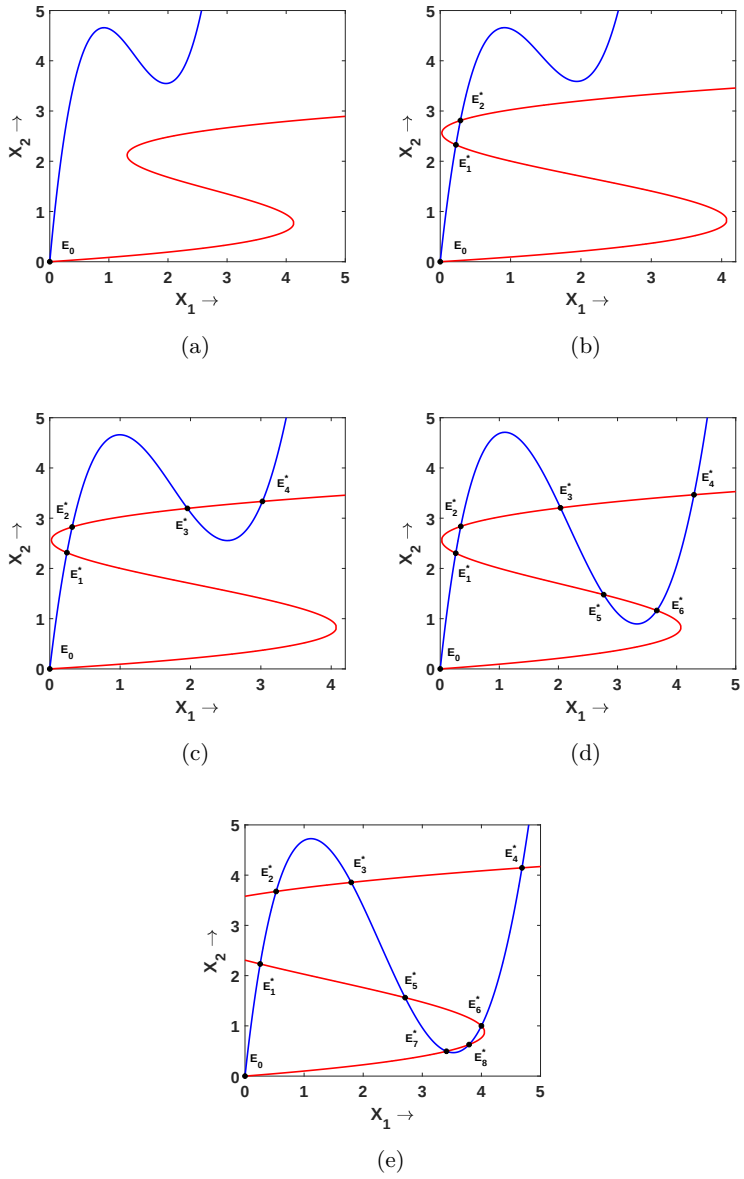

Figure 2: Graphical representation of the prey nullcline of patch 1 (blue colored curve) and the prey nullcline of patch 2 (red colored curve). They can intersect at a maximum of eight points, namely, $E_i^*(X_1^*, X_2^*)$, $i = 1, \ldots, 8$.

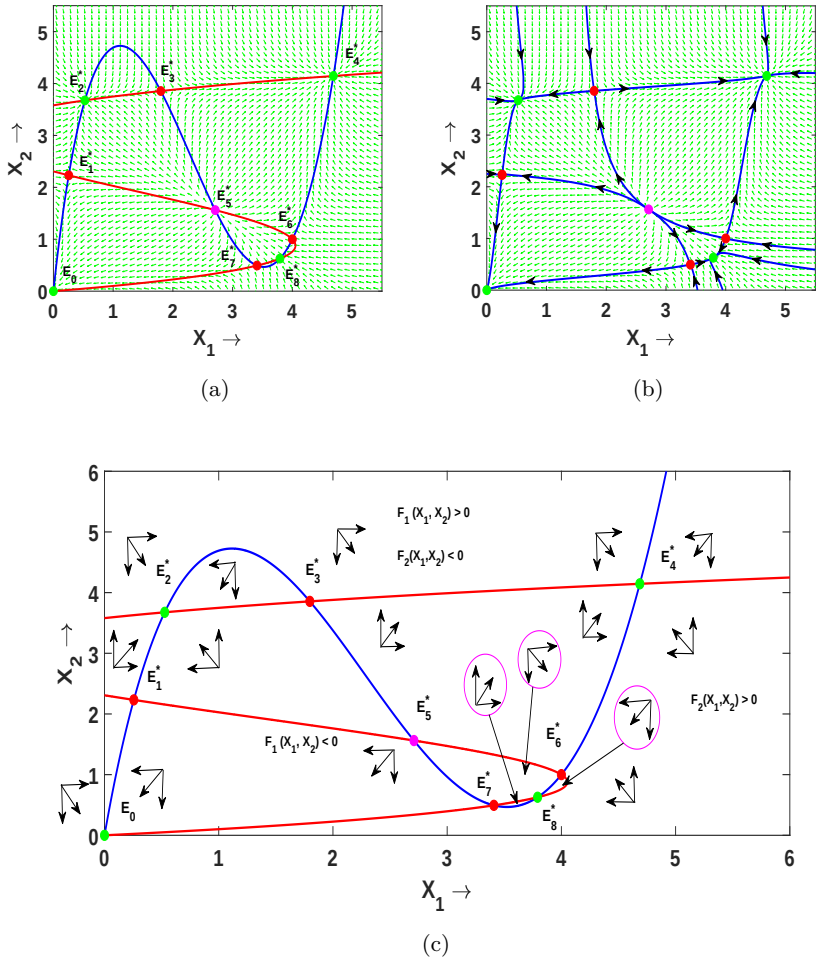

Figure 3: **(a)** Possible number of coexisting equilibrium points; nullclines of X_1 and X_2 are represented by the blue and red solid curves, respectively, **(b)** Position and stability of nine equilibrium points: green, red, and magenta solid points represent stable, saddle, and unstable equilibrium points, respectively, **(c)** Nature of stability of the interior equilibrium point by using direction of vector field.

Assume that $\frac{dX_2}{dX_1}^{(F_1)}$ and $\frac{dX_2}{dX_1}^{(F_2)}$ denote the gradient of the tangent of the curve $F_1(X_1, X_2) = 0$ and $F_2(X_1, X_2) = 0$, respectively. Hence, we may express the determinant of $J_{E_i^*}$ as follows using the implicit function theorem:

$$det(J_{E_i^*}) = \left[\frac{\partial F_1}{\partial X_2}\frac{\partial F_2}{\partial X_2}\left(\frac{dX_2}{dX_1}^{(F_2)} - \frac{dX_2}{dX_1}^{(F_1)}\right)\right]. \tag{5}$$

Now, we will explain how to determine the sign of $[\frac{\partial F_1}{\partial X_1}]_{E_1^*}$. Since $F_1(X_1, X_2) < 0$ below the nontrivial prey nullcline and $F_1(X_1, X_2) > 0$ for the opposite side. Hence when we move from left to the equilibria E_1^* to right sign changes from positive to negative, that is,$F_1(X_1^* - \frac{\Delta X_1}{2}, X_2) > 0$ and $F_1(X_1^* + \frac{\Delta X_1}{2}, X_2) < 0$, which imply that $\frac{\partial F_1}{\partial X_1}|_{E_1^*} < 0$. The signs of the remaining terms in the Jacobian matrix $J_{E_1^*}$ may also be found in a similar manner.

Therefore, we have the sign of the Jacobian matrix J around E_1^* by using the graphical Jacobian method [31, 35] as follows:

$$Sign(J_{E_1^*}) = Sign\begin{bmatrix}\frac{\partial F_1}{\partial X_1} & \frac{\partial F_1}{\partial X_2}\\ \\ \frac{\partial F_2}{\partial X_1} & \frac{\partial F_2}{\partial X_2}\end{bmatrix} = Sign\begin{bmatrix}-\beta_{12}p_1'(X_1^*) & \beta_{21}\\ \beta_{12} & -\beta_{21}p_2'(X_2^*)\end{bmatrix}$$
$$= \begin{bmatrix}- & +\\ + & +\end{bmatrix},$$

and we provide the graphical representation in Figure 3(c). But in this case, $\frac{dX_2}{dX_1}^{(F_1)}\Big|_{E_1^*} > \frac{dX_2}{dX_1}^{(F_2)}\Big|_{E_1^*}$, and expression (5) gives $det(J_{E_1^*}) < 0$, and we also get $p_1'(X_1^*) + p_2'(X_2^*) > 0$, but $p_1'(X_1^*)p_2'(X_2^*) < 0$. Therefore, we can see that the stability requirements (4) are not met in this case, which implies that E_1^* is always a saddle point. □

Similar to this, it is simple to demonstrate the stability of any other interior equilibrium point.

Now, we also consider a numerical example to illustrate the stability of these nine equilibrium points is shown in Figure 3(b). To do this, we have considered the following set of parameter values:

$$\begin{aligned} &r_1 = 4.1, \quad A_1 = 0.95, \quad E_1 = 1.8, \quad b_1 = 1.57, \quad L_1 = 2.3, \quad \beta_{21} = 0.27,\\ &\beta_{12} = 0.2, \quad r_2 = 4.3, \quad A_2 = 0.90, \quad E_2 = 1.2, \quad b_2 = 1.76, \quad L_2 = 1.6,\\ &q_1 = 3.125939754, \quad q_2 = 1.86576534254, \quad K_1 = 5.4, \quad K_2 = 4.6. \end{aligned} \tag{6}$$

For this choice of parameter values, we find the following nine equilibrium points:

$$E_0 = (0,0),\ E_1^* = (0.2566, 2.2320),\ E_2^* = (0.527, 3.675),\ E_3^* = (1.797, 3.856),$$
$$E_4^* = (4.687, 4.145),\ E_5^* = (2.709, 1.562),\ E_6^* = (4,1),\ E_7^* = (3.409, 0.494),$$
$$E_8^* = (3.792, 0.627).$$

Among these nine equilibria, E_0, E_2^*, E_4^*, and E_8^* are always locally asymptotically stable points; E_1^*, E_3^*, E_6^*, and E_7^* are always saddle points; and E_5^* is an unstable node, as shown in Figure 3(b) and summarized in Table 1.

Table 1: Summary of existence and stability of equilibrium points.

Equilibrium points	**Stability**
E_0 (Always exists)	Always locally asymptotically Stable
E_1^*, E_3^*, E_6^*, E_7^* (If exist)	Always a Saddle point
E_2^*, E_{4^*}, E_8^* (If exist)	Always locally asymptotically Stable
E_5^* (If exists)	Always an Unstable point

3.2 Bifurcation structure

As we know, the number of prey in any patch depends on the patch's carrying capacity; therefore, with the aid of bifurcation, we investigate how the dynamical properties of the system will alter as the carrying capacity rises and falls. In our investigation, we have observed that the system exhibits only one local bifurcation, namely, the saddle-node bifurcation or limit point bifurcation (**LP**), which is the local bifurcation of co-dimension one. Saddle-node bifurcation is the process through which two equilibrium points are

simultaneously created or destroyed as the parameter varies, and two equilibrium points collide at the bifurcation threshold, which is shown in Figures 4 and 5. Therefore, many such situations arise where the system becomes monostable, bistable, and tri-stable, as shown in Figures 5, 6, and 7.

3.3 Saddle node bifurcation

We now investigate the saddle-node bifurcation for the system (2) with respect to the carrying capacity of patch 1, that is, K_1. Due to this bifurcation, two interior equilibrium points coincide at a single equilibrium point E^*_{SN}, that is, two nontrivial nullclines touches each other at E^*_{SN} for the threshold value $K^*_{1_{SN}}$. Therefore, $\mathrm{Det}(J_{E^*_{SN}}) = 0$. This means one of the eigenvalue of $(J_{K^*_{1_{SN}}})$ is zero with multiplicity one. Now, we will check the transversality conditions of the Sotomayor theorem [24] for saddle-node bifurcation.

Let V and W be the eigenvectors of $J_{E^*_{SN}}$ and $\left[J_{E^*_{SN}}\right]^T$ corresponding to zero eigenvalue, respectively. Here, $V = \begin{pmatrix} \beta_{21} \\ \beta_{12}p_1'(X_1) \end{pmatrix}$ and $W = \begin{pmatrix} 1 \\ p_1'(X_1) \end{pmatrix}$. By using the technique outlined in [19], the transversality conditions for the saddle-node bifurcation in our system are as follows:

$$W^T F_{K_1}(E^*_{SN}; K^*_{1_{SN}}) = \frac{r_1 A_1 X^*_{1_{SN}}}{K^{2^*}_{1_{SN}}} - \frac{r_1 X^{2^*}_{1_{SN}}}{K^{2^*}_{1_{SN}}} - \frac{2r_1 A_1 X^{2^*}_{1_{SN}}}{K^{3^*}_{1_{SN}}} + \frac{2r_1 X^{3^*}_{1_{SN}}}{K^{3^*}_{1_{SN}}} \neq 0, \tag{7}$$

$$W^T D^2 F(E^*_{SN}; K^*_{1_{SN}})(V, V) = -\beta_{12}\beta^2_{21}p_1''(X_1) - \beta^2_{12}\beta_{21}p_2''(X_2)(p'(X_1))^3 \neq 0. \tag{8}$$

Due to the difficulty in determining the exact expression of E^*_{SN} analytically, we use a numerical example to verify if saddle-node bifurcation occurs. Therefore, we will perform a numerical evaluation of the transversality conditions (7) and (8). So here, we choose the saddle node bifurcation curve 1 (SN_1) to quantitatively test all these conditions. For $K_1 = 2.9$ and $K_2 = 4.615$ and all other parameters are fixed at (6), we start from the region R_{11} of Figure 4, where the system (2) has four interior equilibrium points E^*_1, E^*_2, E^*_3, and E^*_4. When K_1 continuously decreases and reaches its threshold value $K^*_{1_{SN_1}} = 2.6799535268$, we have observed that third and fourth interior equilibrium points coincide; that is,

$E_3^* = E_4^* = (1.779209934, 3.867745878) = E^*_{SN_1}(X^*_{1_{SN_1}}, X^*_{2_{SN_1}})$. We have also observed that if we reduce K_1's value further after it reaches its threshold value, the system has just two interior equilibrium points E_1^* and E_2^*. For the saddle-node bifurcation curve 1, that is, SN_1 (the magenta-colored curve in Figure 4), the transversality conditions are $w^T F_{K_1}(E^*_{SN_1}; K^*_{1_{SN_1}}) = 0.276069791(\neq 0)$, $w^T D^2F(E^*_{SN_1}; K^*_{1_{SN_1}})(V,V) = -0.1264730496(\neq 0)$, and $\text{Det}(J(X^*_{1_{SN_1}}, X^*_{2_{SN_1}}))|_{K^*_{1_{SN_1}}} = 0$. This indicates that all the necessary conditions for SN_1 to occur are satisfied. Similarly, we can easily verify these transversality conditions (7) and (8) for all other saddle-node bifurcation curves.

3.3.1 Two parameter bifurcation

In this subsection, we are interested in studying the effect of K_1 and K_2 on system dynamics. So, we perform the bifurcation analysis for the simultaneously changing values of K_1 and K_2, and their corresponding results are summarized in Table 2. In Figure 4, we present the bifurcation diagram in the K_1K_2-parametric plane and explain how the local bifurcation curves divide the entire parametric plane into different subregions, each of which exhibits the system's dynamical behavior in a qualitatively distinct way. From this figure, we have observed that the saddle-node bifurcation curves SN_2 and SN_6 coincide at a point that is marked with a black bubble known as the cusp point (**CP**). Therefore, at the existence of this point, three equilibrium points coincide into a single equilibrium point.

3.3.2 One parameter bifurcation

We are focused here on understanding how the carrying capacity affects the species population. In order to do so, we provide two one-parametric bifurcation diagrams (see Figures 5(a) and 5(b)) with respect to K_1 and all other parameter values are fixed at (6). Figure 5 demonstrates that the number of interior equilibrium points in the system either rises or falls pairwise as the carrying capacity K_1 grows. Our system has seven saddle-node bifurcation

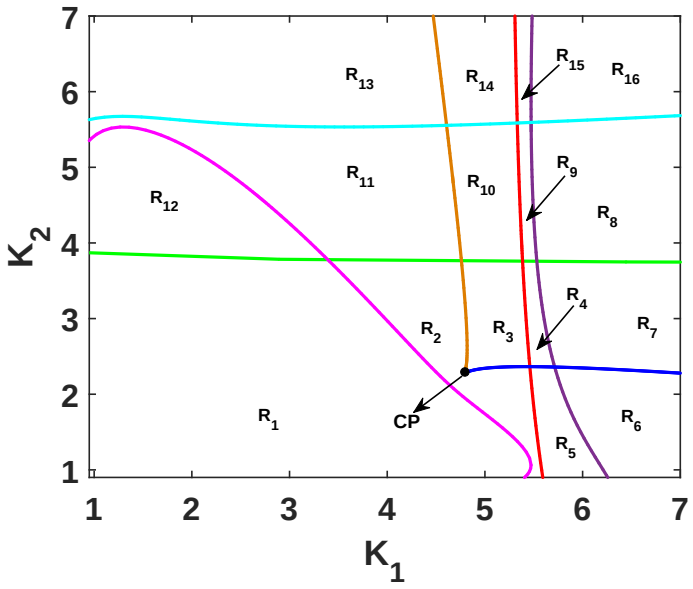

Figure 4: Two parameter bifurcation diagram in K_1K_2-plane. Black bubble represents cusp point and with reference to this point, the equilibrium points E_3^*, E_5^*, and E_6^* coincide at E_6^*.

curves, denoted by SN_i, $i = 1, \ldots, 7$, which are depicted in Figure 4 and summarized in Table 2. Among these seven curves, we will concentrate only on the four curves, SN_i, $i = 1, \ldots, 4$.

From Figures 5(a) and 5(b), we have observed that the number of interior equilibrium points varies from 2 to 8 and 0 to 4, respectively, but the characteristics of these two figures are quite similar. For this reason, we only describe Figure 5(a) precisely. From this figure, we have observed that for four different K_1 values, there are four **LP** points from which two branches of equilibria emerge. When carrying capacity K_1 is lesser than $K_1^{SN_1} \approx 2.697$, the system has two interior equilibrium points. Furthermore, if we increase the value of K_1 from it, we have observed that the system has four interior equilibrium points. After that, the system exhibits six interior equilibrium points when the value of K_1 lies between $K_1^{SN_2} \approx 4.692$ and $K_1^{SN_3} \approx 5.356$. Finally, when K_1 becomes larger than 5.356, the system reaches the region where the number of interior equilibrium points is at its maximum, which is

Table 2: Saddle-node bifurcations and related equilibrium points.

Serial No.	**Saddle-node bifurcation curves**	**Equilibrium points coincide**
1	SN_1 (Magenta)	E_3^*, E_4^*
2	SN_2 (Brown)	E_5^*, E_6^*
3	SN_3 (Red)	E_7^*, E_8^*
4	$SN4$ (Violet)	E_6^*, E_8^*
5	SN_5 (Green)	E_1^*, E_2^*
6	SN_6 (Blue)	E_3^*, E_5^*
7	SN_7 (Cyan)	E_2^*, E_3^*

equal to 8. In this region, the system has three stable equilibria among eight equilibria, so the system becomes tri-stable. It is also found that, when the carrying capacity exceeds the value $K_1^{SN_4} \approx 5.489$, six interior equilibrium points remain in the system.

Here, we have observed that two bifurcations, SN_1 and SN_4, of the system behave like catastrophic bifurcations. A bifurcation is where the stability of an equilibrium fails, a catastrophe happens, and the system shifts abruptly into a different state. As a result, the system's present stable state vanishes, and it is compelled to transition to an alternate stable state. For SN_1 (catastrophic bifurcation 1), the system instantly switches from stable state E_4^* to E_2^*, and for SN_4 (catastrophic bifurcation 2), the system switches from stable state E_8^* to E_2^*, as illustrated in Figure 5(a).

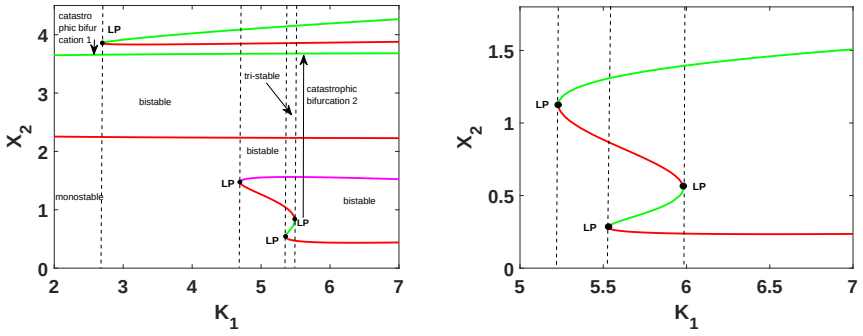

(a) K_2=4.6 (b) K_2=1.5

Figure 5: One parameter bifurcation diagram in K_1X_2-plane. "LP" represents Saddle-node bifurcation. Green, magenta, and red-colored curves represent stable, unstable, and saddle equilibria, respectively.

Let us now describe how the dynamics of the system change mainly for the interior equilibrium points as the parameters move through the different subregions shown in Figure 4. All the phase portraits corresponding to the different subregions of Figure 4 are presented in Figures 6 and 7, in which green, red, and magenta bubbles represent stable, unstable, and saddle points, respectively. Table 3 summarizes the number and type of equilibrium points discovered in various regions of Figure 4, as illustrated in Figures 6 and 7.

4 Stochastic model

Stochasticity plays a crucial role in every living system [8]. In the environment, individuals are born, die, harvested, and dispersed from one place to another at random. As a result, the variability in the aforementioned demographic parameters causes fluctuations in the total size of the individuals, and the associated stochasticity is known as demographic stochasticity. Stochastic models deal with stochasticity (either demographic or environmental) and hence give varying outputs for each input [20]. To study the effect of demographic stochasticity on the population of any individual, we formulate an

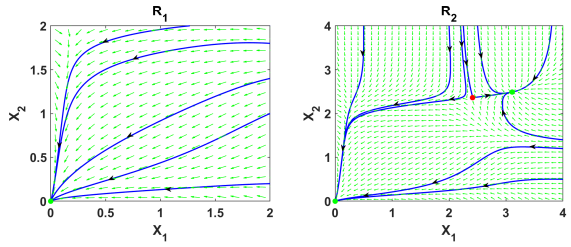

(a) K_1=$K_2 = 3$

(b) $K_1 = 4.2$, $K_2 = 3$

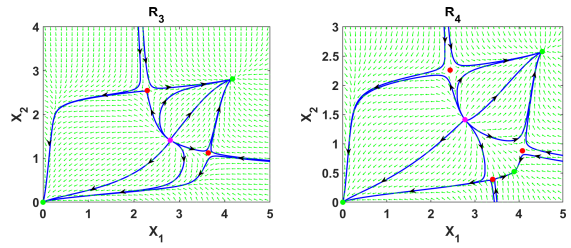

(c) $K_1 = 5.1$, $K_2 = 3.2$

(d) $K_1 = 5.5$, $K_2 = 2.9$

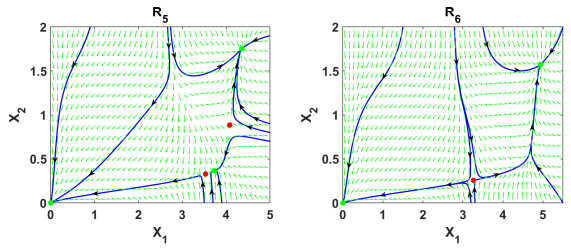

(e) $K_1 = 5.5$, $K_2 = 2$

(f) $K_1 = 6.1$, $K_2 = 1.7$

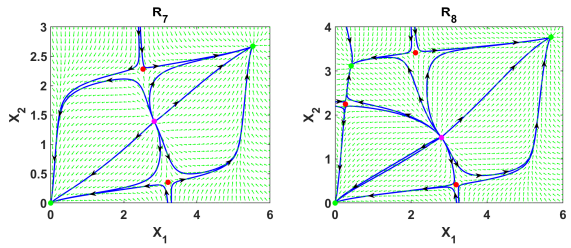

(g) $K_1 = 6.5$, $K_2 = 2.9$

(h) $K_1 = 6.5$, $K_2 = 4.1$

Figure 6: Phase portraits of different regions of Figure 4 are shown for various values of K_1 and K_2, all other parameter values remain same.

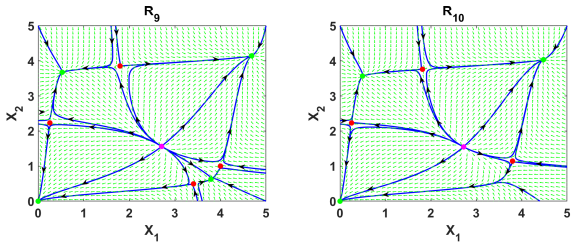

(a) $K_1 = 5.4$, $K_2 = 4.6$ (b) $K_1 = 5.2$, $K_2 = 4.5$

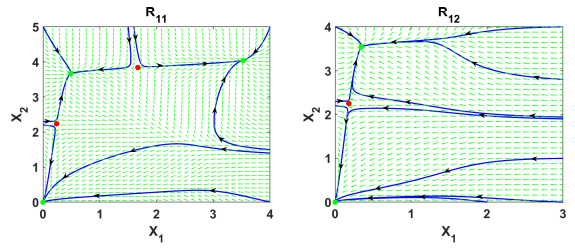

(c) $K_1 = 4.2$, $K_2 = 4.6$ (d) $K_1 = 2$, $K_2 = 4.5$

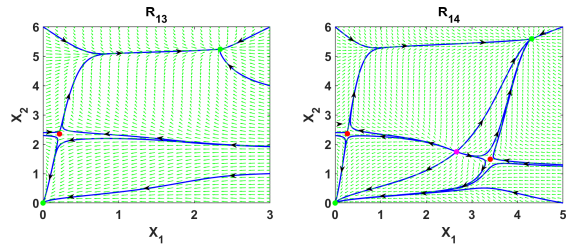

(e) $K_1 = 2.7$, $K_2 = 6$ (f) $K_1 = 4.8$, $K_2 = 6.2$

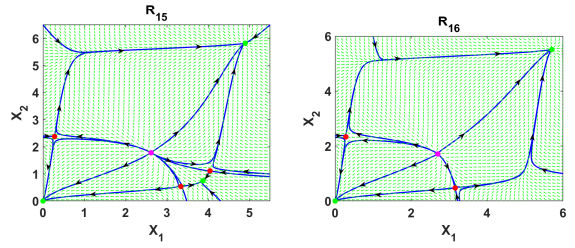

(g) $K_1 = 5.4$, $K_2 = 6.4$ (h) $K_1 = 6.3$, $K_2 = 6$

Figure 7: Phase portraits of different regions of Figure 4 are shown for various values of K_1 and K_2, all other parameter values remain same.

Table 3: Summary of the number of equilibrium points corresponding to the different regions of the bifurcation diagram represented in Figure 4.

Domain	$\mathbf{R_1}$	$\mathbf{R_2}$	$\mathbf{R_3}$	$\mathbf{R_4}$	$\mathbf{R_5}$	$\mathbf{R_6}$
Number of Interior equilibrium point	Nil	E_3^*, E_4^* or, E_4^*, E_6^*	E_3^*, E_4^*, E_5^*, E_6^*	E_3^*, E_4^*, E_5^*, E_6^*, E_7^*, E_8^*	E_4^*, E_6^*, E_7^*, E_8^*	E_4^*, E_7^*

Domain	$\mathbf{R_7}$	$\mathbf{R_8}$	$\mathbf{R_9}$	$\mathbf{R_{10}}$	$\mathbf{R_{11}}$	$\mathbf{R_{12}}$
Number of Interior equilibrium point	E_3^*, E_4^*, E_5^*, E_7^*,	E_1^*, E_2^* E_3^*, E_4^* E_5^*, E_7^*	E_1^*, E_2^* E_3^*, E_4^* E_5^*, E_6^* E_7^*, E_8^*	E_1^*, E_2^* E_3^*, E_4^* E_5^*, E_6^*	E_1^*, E_2^*, E_3^*, E_4^*	E_1^*, E_2^*

Domain	$\mathbf{R_{13}}$	$\mathbf{R_{14}}$	$\mathbf{R_{15}}$	$\mathbf{R_{16}}$
Number of Interior equilibrium point	E_1^*, E_4^*,	E_1^*, E_4^* E_5^*, E_6^*	E_1^*, E_4^*, E_5^*, E_6^*, E_7^*, E_8^*	E_1^*, E_4^* E_5^*, E_7^*

Note: The stability nature of all equilibrium points corresponding to the different regions of bifurcation diagram (Figure 4) remains the same, which is already illustrated in Table 1.

equivalent stochastic model of our ordinary differential equation model (2) using the CTMC modeling approach [2, 5, 4, 3, 18, 20, 13]. For the sake of simplicity, we have considered the same notations for the random variables as in the deterministic model. Let $X_i(t)$ stand for the discrete random variable that represents the number of prey at time t presenting within a patch i. As the number of prey in any patch depends on the carrying capacity of the patch and the probability of occurrence of every event in the stochastic process depends on the number of prey, we can argue that the carrying capacity is essential for the variability in the stochastic processes. Let $X_i(t) \in \{0, 1, 2, \ldots, G\}$ be the random variables, where G is constant and

$t \in \mathbb{R}_+$. Assume that $\{(X_1(t), X_2(t)) : t \in [0, \infty)\}$ is a bivariate homogeneous Markov process with a probability function

$$p_{(x_1,x_2)(t)} = \text{Prob}(X_1(t) = x_1, X_2(t) = x_2). \tag{9}$$

Table 4: State transitions and rates describing the stochastic model.

Description	**Transition**	**Rate**
Birth of X_1	$(X_1, X_2) \to (X_1 + 1, X_2)$	$r_1 X_1 \left(\frac{X_1}{K_1} - \frac{A_1}{K_1}\right) \left(1 - \frac{X_1}{K_1}\right)$
Birth of X_2	$(X_1, X_2) \to (X_1, X_2 + 1)$	$r_2 X_2 \left(\frac{X_2}{K_2} - \frac{A_2}{K_2}\right) \left(1 - \frac{X_2}{K_2}\right)$
Death of X_1 due to harvesting	$(X_1, X_2) \to (X_1 - 1, X_2)$	$\frac{q_1 E_1 X_1}{b_1 E_1 + L_1 X_1}$
Death of X_2 due to harvesting	$(X_1, X_2) \to (X_1, X_2 - 1)$	$\frac{q_2 E_2 X_2}{b_2 E_2 + L_2 X_2}$
Dispersal of X_2 from patch 2 to patch 1	$(X_1, X_2) \to (X_1 + 1, X_2 - 1)$	$\beta_{21} X_2$
Dispersal of X_1 from patch 1 to patch 2	$(X_1, X_2) \to (X_1 - 1, X_2 + 1)$	$\beta_{12} X_1$

Let $\Delta X_i(t) \equiv X_i(t + \Delta t) - X_i(t)$ and Δt be sufficiently small such that $\Delta X_i \in \{-1, 0, 1\}$ for $i = 1, 2$. The transition probabilities listed below are defined for a short time interval Δt using the state transition rates listed in Table 4:

(i) While there is no birth or death of X_2, the likelihood of X_1 being born is $r_1 x_1 \left(\frac{x_1}{K_1} - \frac{A_1}{K_1}\right) \left(1 - \frac{x_1}{K_1}\right) \Delta t + o(\Delta t)$.

(ii) While there is no birth or death of X_1, the likelihood of X_2 being born is $r_2 x_2 \left(\frac{x_2}{K_2} - \frac{A_2}{K_2}\right) \left(1 - \frac{x_2}{K_2}\right) \Delta t + o(\Delta t)$.

(iii) The probability of X_1 dying as a result of harvesting is $\frac{q_1 E_1 x_1}{b_1 E_1 + L_1 x_1} \Delta t + o(\Delta t)$.

(iv) Due to harvesting, X_2 dies with probability $\frac{q_2 E_2 x_2}{b_2 E_2 + L_2 x_2} \Delta t + o(\Delta t)$.

(v) The probability of dispersal of X_2 from patch 2 to patch 1 is $\beta_{21}x_2\Delta t + o(\Delta t)$.

(vi) X_1 disperses from patch 1 to patch 2 with probability $\beta_{12}x_1\Delta t + o(\Delta t)$.

(vii) The probability of the system having no births, deaths, or dispersal is $1 - \Big[r_1x_1\left(\frac{x_1}{K_1} - \frac{A_1}{K_1}\right)\left(1 - \frac{x_1}{K_1}\right) + r_2x_2\left(\frac{x_2}{K_2} - \frac{A_2}{K_2}\right)\left(1 - \frac{x_2}{K_2}\right) + \frac{q_1E_1x_1}{b_1E_1+L_1x_1} + \frac{q_2E_2x_2}{b_2E_2+L_2x_2} + \beta_{21}x_2 + \beta_{12}x_1\Big]\Delta t + o(\Delta t)$.

Therefore, the transition probabilities from state (x_1, x_2) to state $(x_1 + j_{x_1}, x_2 + j_{x_2})$ are as follows:

$$p_*(\Delta t) = \begin{cases} r_1x_1\left(\frac{x_1}{K_1} - \frac{A_1}{K_1}\right)\left(1 - \frac{x_1}{K_1}\right)\Delta t & \\ +o(\Delta t), & (j_{x_1}, j_{x_2}) = (1,0), \\ r_2x_2\left(\frac{x_2}{K_2} - \frac{A_2}{K_2}\right)\left(1 - \frac{x_2}{K_2}\right)\Delta t & \\ +o(\Delta t), & (j_{x_1}, j_{x_2}) = (0,1), \\ \frac{q_1E_1x_1}{b_1E_1+L_1x_1}\Delta t + o(\Delta t), & (j_{x_1}, j_{x_2}) = (-1,0), \\ \frac{q_2E_2x_2}{b_2E_2+L_2x_2}\Delta t + o(\Delta t), & (j_{x_1}, j_{x_2}) = (0,-1), \\ \beta_{21}x_2\Delta t + o(\Delta t), & (j_{x_1}, j_{x_2}) = (1,-1), \\ \beta_{12}x_1\Delta t + o(\Delta t), & (j_{x_1}, j_{x_2}) = (-1,1), \\ 1 - \Big[r_1x_1\left(\frac{x_1}{K_1} - \frac{A_1}{K_1}\right)\left(1 - \frac{x_1}{K_1}\right) & \\ +r_2x_2\left(\frac{x_2}{K_2} - \frac{A_2}{K_2}\right)\left(1 - \frac{x_2}{K_2}\right) & \\ +\frac{q_1E_1x_1}{b_1E_1+L_1x_1} + \frac{q_2E_2x_2}{b_2E_2+L_2x_2} + \beta_{21}x_2 & \\ +\beta_{12}x_1\Big]\Delta t + o(\Delta t), & (j_{i_h}, j_{i_m}) = (0,0), \\ o(\Delta t), & otherwise, \end{cases} \tag{10}$$

where $p_*(\Delta t) = p_{(x_1+j_{x_1}, x_2+j_{x_2}),(x_1,x_2)}(\Delta t)$, and $o(\Delta t)$ has the following property:

$$\lim_{\Delta t \to 0} \frac{o(\Delta t)}{\Delta t} = 0.$$

The probabilities $p_{(x_1,x_2)}(t)$ satisfy the following forward Kolmogorov differential equation:

$$\frac{dp_{(x_1,x_2)}(t)}{dt} = \Phi_1(x_1 - 1, x_2)p_{(x_1-1,x_2)}(t) + \Psi_1(x_1 + 1, x_2)p_{(x_1+1,x_2)}(t)$$

$$
\begin{aligned}
&+ \Phi_2(x_1, x_2 - 1)p_{(x_1,x_2-1)}(t) + \Psi_2(x_1, x_2 + 1)p_{(x_1,x_2+1)}(t) \\
&+ \Upsilon_1(x_1 - 1, x_2 + 1)p_{(x_1-1,x_2+1)}(t) \\
&+ \Upsilon_2(x_1 + 1, x_2 - 1)p_{(x_1-1,x_2+1)}(t) - \Omega(x_1, x_2)p_{(x_1,x_2)}(t),
\end{aligned} \tag{11}
$$

$$
\begin{aligned}
\text{where} \quad \Phi_1(x_1, x_2) &= r_1 x_1 \left(\frac{x_1}{K_1} - \frac{A_1}{K_1}\right)\left(1 - \frac{x_1}{K_1}\right), \\
\Phi_2(x_1, x_2) &= r_2 x_2 \left(\frac{x_2}{K_2} - \frac{A_2}{K_2}\right)\left(1 - \frac{x_2}{K_2}\right), \\
\Psi_1(x_1, x_2) &= \frac{q_1 E_1 x_1}{b_1 E_1 + L_1 x_1}, \\
\Psi_2(x_1, x_2) &= \frac{q_2 E_2 x_2}{b_2 E_2 + L_2 x_2}, \\
\Upsilon_1(x_1, x_2) &= \beta_{21} x_2, \\
\Upsilon_1(x_1, x_2) &= \beta_{12} x_1, \\
\Omega(x_1, x_2) &= (\Phi_1 + \Phi_2 + \Psi_1 + \Psi_2 + \Upsilon_1 + \Upsilon_2).
\end{aligned} \tag{12}
$$

Equation (11) also known as the Master equation. Solving this equation analytically is challenging for us. Therefore, we employ the Gillespie algorithm [9] (see Appendix A) to simulate the relevant stochastic model of the bivariate process in order to generate sample paths (stochastic realisations) for the process.

4.1 Comparison between deterministic and stochastic model

In this part, we show the possibility of population extinction in a finite amount of time for different carrying capacities (values are given in the caption of the graph) by comparing the sample paths of the stochastic model to the numerical solution of the deterministic model (see Figures 8(a) and 8(b)). To do this, we take the initial conditions $X_1(0) = 4$, $X_2(0) = 1$, and the parameter values $r_1 = 4.1$, $A_1 = 0.95$, $E_1 = 1.8$, $b_1 = 1.57$, $L_1 = 2.3$, $\beta_{21} = 0.27$, $\beta_{12} = 0.2$, $r_2 = 4.3$, $A_2 = 0.90$, $E_2 = 1.2$, $b_2 = 1.76$, $L_2 = 1.6$, $q_1 = 3.125939754$, $q_2 = 1.86576534254$. Sample paths in Figures 8(a) and

8(b) hit the time axis in a finite amount of time, depicting the extinction of the populations, whereas the deterministic solution (red solid curve) depicts the existence of the populations. From these figures, we also see that carrying capacity has no impact on population extinction or existence but slightly affects extinction time.

In Figures 9(a) and 9(c), we plot the stochastic trajectories for the system (11) by taking into account the initial number of individuals in the domain of attraction of the stable equilibrium points (E_0 and E_{2^*}) in order to better understand the possibility of population extinction in the presence of demographic stochasticity. In Figures 9(b) and 9(d), the relevant time series is presented. According to Figure 9(a), when the initial population is in the region of attraction of E_0, the deterministic trajectory reaches E_0 (see dashed magenta curve), which indicates population extinction, but when stochasticity is present, two cases occur: among three trajectories, one reaches E_0 (see dashed green curve), which shows population extinction, and the other two trajectories are concentrated in the region of attraction of E_0, that is, the existence of individuals in the population. The Gillespie algorithm [9] and 10,000 sample paths are used to assess the chance of population extinction. In this scenario, the estimated probability of population extinction is 0.7589. In Figure 9(b), these two possibilities for the stochastic model are illustrated.

Additionally, when we consider the initial number of population in the domain of attraction of E_{2^*} (see Figure 9(c)), we notice that the deterministic trajectory (solid magenta curve) depicts the existence of individuals in the population, whereas the stochastic trajectory depicts two possible outcomes: among three trajectories, one is concentrated in the domain of attraction of E_{2^*}, and the other two (dashed green curve) cross the separatrix and enter the domain of attraction of E_0, finally reaching E_0. These two scenarios of the stochastic model demonstrate that either individuals remain in the population or they disappear. These two possibilities of the stochastic model are depicted in Figure 9(d). In this case, the probability of population extinction is 0.5673.

Figure 10 also shows how demographic stochasticity affects the persistence of the species in the population by comparing the results of the deterministic and stochastic models for varying numbers of initially existing individuals in

the basin of attraction of equilibrium point E_{4^*}. From this figure, we have observed that the stochastic model always shows the only extinction of the second prey species from the population (shown by the sample paths that hit the x-axis), whereas the deterministic model always shows the persistence of both prey species (shown by the magenta solid curve) when the initial number of prey in the population is within the domain of attraction of the stable equilibrium point E_{4^*}. The parameter values are listed in (6). The caption of each subfigure of Figure 10 indicates the number of individuals initially present in the population.

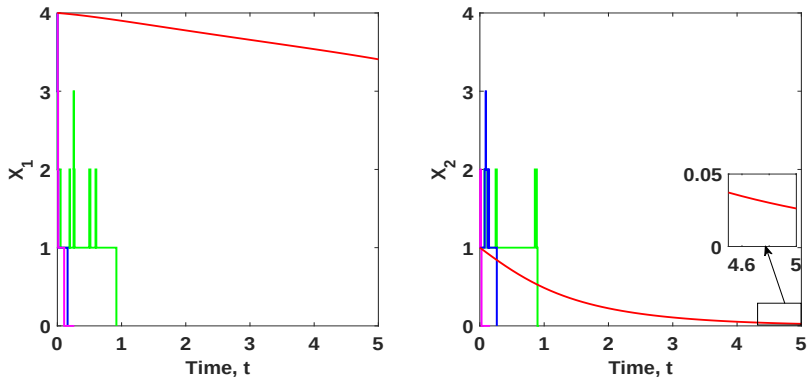

(a)

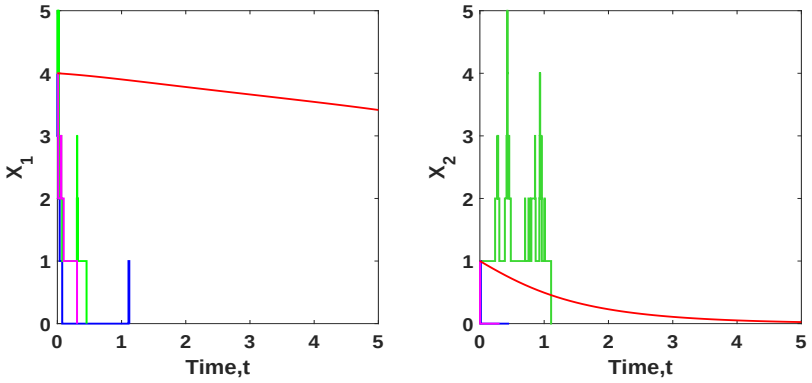

(b)

Figure 8: For varied carrying capacity of the patches, three sample paths of the stochastic model and the corresponding deterministic solution (red solid curve) of model (2). In **(a)** $K_1 = 5.4$, $K_2 = 4.6$, and in **(b)** $K1 = K_2 = 5.4$.

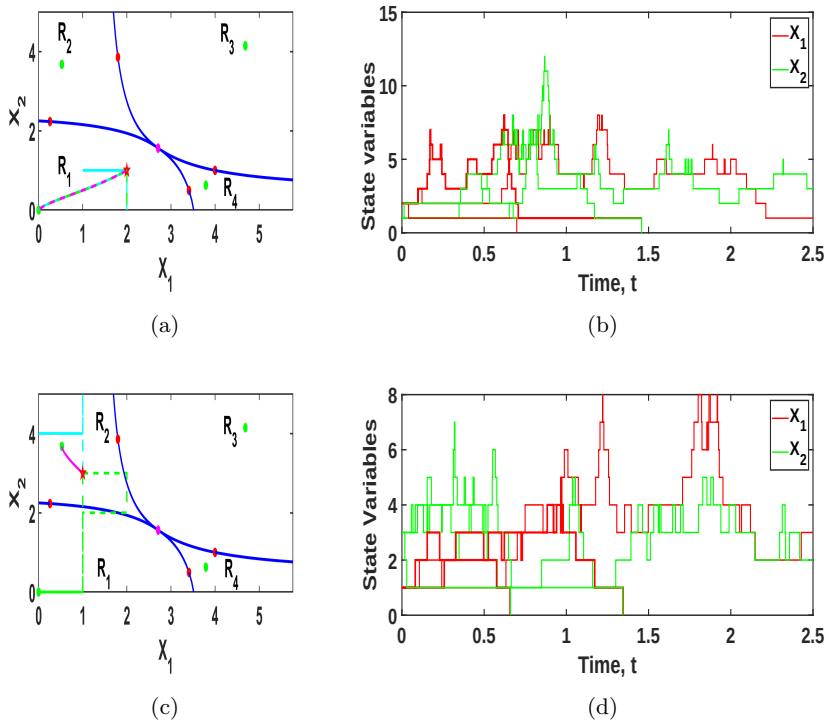

Figure 9: In **(a)** and **(b)** stochastic trajectories starting near E_0 and E_2^*, respectively. Green, red, and magenta solid points represent stable, saddle, and unstable equilibrium points, respectively. The initial point is symbolized by the red star. Separatrix is represented by blue solid line. Magenta-colored line represents the deterministic trajectory, and the remaining curves represent the stochastic model's sample paths, in both **(a)** and **(b)**. In **(c)** and **(d)** time series with X_1 in red and X_2 in green. Initial condition: in **(a)** and **(b)** $X_1 = 2, X_2 = 1$, and in **(c)** and **(d)** $X_1 = 1, X_2 = 3$. Parameter values are listed in (6).

4.2 Expected time to population extinction

The expected time to population extinction is the amount of time it will take for a system to eliminate individuals from the system [2, 20]. The generator matrix $Q = (q_{ji})$ can be used to estimate this, where the transition rate from state i to state j is represented by q_{ji} $(i, j = 0, 1, 2, \ldots)$. Transition

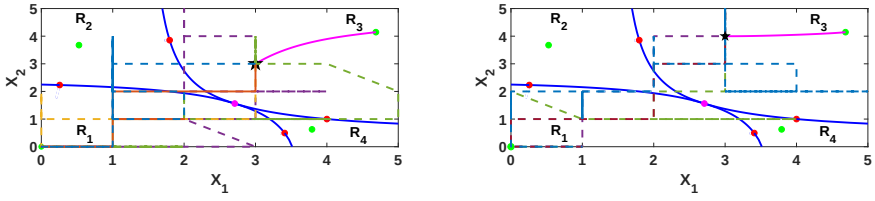

(a) $X_1 = 3,\ X_2 = 3$

(b) $X_1 = 3,\ X_2 = 4$

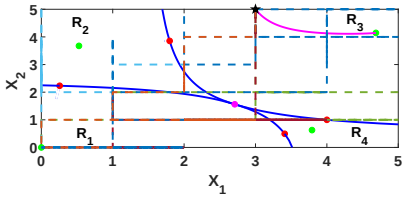

(c) $X_1 = 3,\ X_2 = 5$

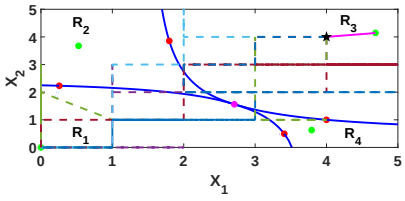

(d) $X_1 = 4,\ X_2 = 4$

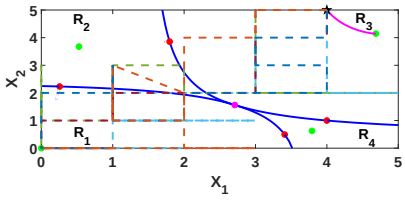

(e) $X_1 = 4,\ X_2 = 5$

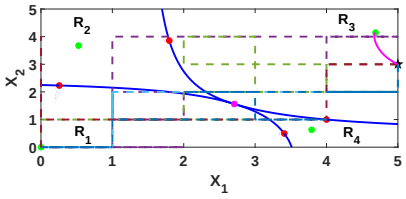

(f) $X_1 = 5,\ X_2 = 3$

Figure 10: Five stochastic trajectories (dashed curves) and the corresponding deterministic solution (solid magenta curve) of the two patch model (2). Green, red, and magenta solid points represent stable, saddle, and unstable equilibrium points, respectively. The initial point is symbolized by the black pentagram. Separatrix is represented by blue solid line. Parameter values are listed in (6). Each subfigure's caption provides an initial number of individuals.

probabilities p_{ji} are used to compute transition rates q_{ji} [20]. The following formula can be used to get the generator matrix Q from the infinitesimal transition matrix $P(\Delta t) = (p_{ji}(\Delta t))$:

$$Q = \lim_{\Delta t \to 0^+} \frac{P(\Delta t) - \mathbb{I}}{\Delta t}, \tag{13}$$

where p_{ji} represents probability of transition from state i to state j, and $\mathbb{I}$ stands for the same-dimensional matrix (the identity matrix in the finite

case), which has zeros everywhere and ones along the diagonal. Assume that the transition probabilities $p_{ji}(t)$ are continuous and differentiable for $t \geq 0$ [2, 20]. Initially, $p_{ji} = 0$, $i \neq j$ and $p_{ii} = 1$. To calculate the time evolution of the transition probabilities, use the following formula:

$$\frac{dp}{dt} = Qp, \tag{14}$$

where $Q = (q_{ji})$ can be expressed as

$$\begin{pmatrix} q_{00} & q_{01} & q_{02} & \cdots \\ q_{10} & q_{11} & q_{12} & \cdots \\ q_{20} & q_{21} & q_{22} & \cdots \\ \vdots & \vdots & \vdots & \ddots \end{pmatrix}. \tag{15}$$

The following formula can be used to estimate the amount of time before population extinction [2]:

$$\tau = c\tilde{Q}^{-1}, \tag{16}$$

where $c = \underbrace{(-1, -1, \ldots, -1)}_{(X_1 \times X_2)-\text{times}}$ and $\tilde{Q}$ is generated by removing the generator matrix's first row and first column. Equation (11) can be expressed in the matrix form as follows:

$$\frac{dp}{dt} = Qp, \tag{17}$$

where the generator matrix $Q = (q_{ji}) \in M_{(X_1+1)(X_2+1)\times(X_1+1)(X_2+1)}(\mathbb{R})$ and the total number of prey in patch i is X_i, $i = 1, 2$. In the finite state space, we have

$$Q = \begin{pmatrix} W_0 & Z_1 & 0 & \ldots & 0 & 0 \\ Y_0 & W_1 & Z_2 & \ldots & 0 & 0 \\ \vdots & \vdots & \vdots & \ddots & \vdots & \vdots \\ 0 & 0 & 0 & \ldots & W_{X_1-1} & Z_{X_1} \\ 0 & 0 & 0 & \ldots & Y_{X_1-1} & W_{X_1} \end{pmatrix}, \tag{18}$$

where W_s, Y_s, $Z_s \in M_{(X_2+1)\times(X_2+1)}(\mathbb{R})$, and

$$W_s = \begin{pmatrix} -\Omega(s,0) & \Psi_2(s,1) & 0 & \dots & 0 & 0 \\ \Phi_2(s,0) & -\Omega(s,1) & \Psi_2(s,2) & \dots & 0 & 0 \\ \vdots & \vdots & \vdots & \ddots & \vdots & \vdots \\ 0 & 0 & 0 & \dots & -\Omega(s,X_2-1) & \Psi_2(s,X_2) \\ 0 & 0 & 0 & \dots & \Phi_2(s,X_2-1) & -\Omega(s,X_2) \end{pmatrix},$$

$$Y_s = \begin{pmatrix} \Phi_1(s,0) & \Upsilon_1(s,1) & 0 & \dots & 0 & 0 \\ 0 & \Phi_1(s,1) & \Upsilon_1(s,2) & \dots & 0 & 0 \\ \vdots & \vdots & \vdots & \ddots & \vdots & \vdots \\ 0 & 0 & 0 & \dots & \Phi_1(s,X_2-1) & \Upsilon_1(s,X_2) \\ 0 & 0 & 0 & \dots & 0 & \Phi_1(s,X_2) \end{pmatrix},$$

$$Z_s = \begin{pmatrix} \Psi_1(s,0) & 0 & 0 \dots & 0 & 0 \\ \Upsilon_2(s,0) & \Psi_1(s,1) & 0 \dots & 0 & 0 \\ \vdots & \vdots & \vdots \ddots & \vdots & \vdots \\ 0 & 0 & 0 \dots & \Psi_1(s,X_2-1) & 0 \\ 0 & 0 & 0 \dots & \Upsilon_2(s,X_2-1) & \Psi_1(s,X_2) \end{pmatrix},$$

where $s = 0, 1, \dots, X_1$.

4.2.1 Effect of K_1 and K_2 on expected time to population extinction

In this section, we look into how carrying capacity can affect the time it takes for species to go extinct. In this scenario, we take into account the following three possibilities: $K_1 = K_2$, $K_1 < K_2$, and $K_2 > K_1$. The same parameter values and initial conditions as in subsection 4.1 have been employed in this analysis. Figures 11(a) and 11(b) demonstrate that the time required for extinction of the species is reduced when $K_1 > K_2$, as compared to the cases where $K_1 = K_2$ and $K_1 < K_2$. This leads us to the conclusion that K_1 has a more significant effect on the extinction time than K_2.

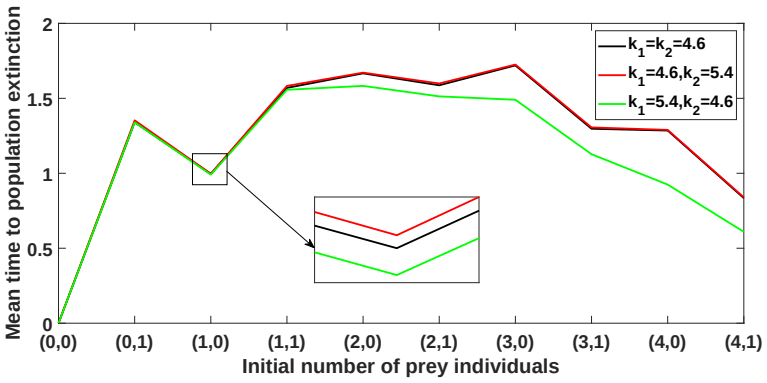

(a)

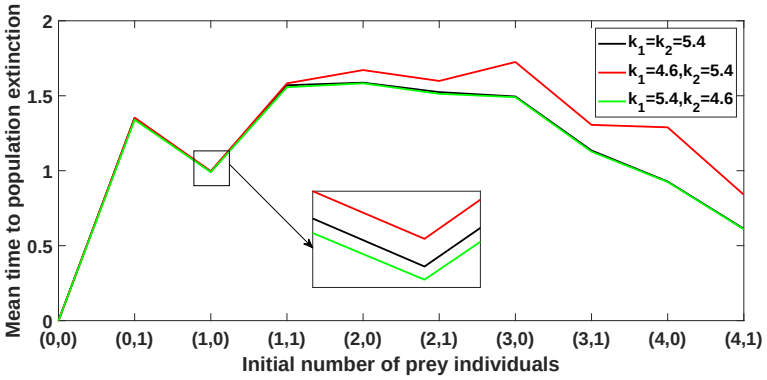

(b)

Figure 11: Effect of different carrying capacities on expected time to population extinction.

5 Discussion

The term "carrying capacity" refers to the highest population of a species that an environment can sustain. Numerous limiting factors, including the availability of food, the environment, predators, and competition for resources, have an impact on it. However, it is essential to note that the relationship between carrying capacity and the dynamics of a two-patch system is not simple. Therefore, we are primarily interested in observing the effects of

carrying capacities on the species population in a patchy environment in the absence and presence of randomness.

In this investigation, we have modified a theta logistic model by incorporating nonlinear harvesting and the dispersal of individuals between patches in a patchy environment. After that, we formulated an analogous stochastic model of our modified model by employing the CTMC modeling approach. For the stochastic model, we have derived an implicit equation for the expected time to population extinction. Finally, we numerically studied the possibility of species extinction by using the Gillespie algorithm (see Appendix A) and the effect of the carrying capacities on the population's extinction time. As far as we know, there has been no previous research on the dynamics of our modified theta logistic model with demographic stochasticity. To address this aspect, we have introduced the Gillespie algorithm with Monte Carlo direct method. The detailed advantages of this method over the conventional methods are discussed in Appendix A.

Initially, when both patches have low carrying capacities, we see that there are no species in the system (see Figure 5(b)). As the carrying capacity increases, the population can grow and stabilize at a steady state with maximum population density. It is also observed that if we increase the carrying capacity of both patches simultaneously, there is a specific region, R_9, in which the system exhibits multiple stable states (see Figure 7(a)). The presence of multiple stable states is leading to regime shifts, which are sudden and dramatic changes in ecosystem structure and function. Furthermore, it becomes clear that the number of steady states in the system will fluctuate when the carrying capacity of patches varies, but there is a possibility of the existence of some stable steady states (see Figure 5). Therefore, we can draw the conclusion that, in the absence of demographic stochasticity, the population in both patches will not vanish.

Indeed, there is a possibility of the extinction of species in the presence of demographic stochasticity (see Figure 8), which is the major difference between both deterministic and stochastic models. Figure 9 illustrates the possibility for a demographic stochasticity-induced transition from any other state where both species coexist to the species-free state, and their corresponding time series plot is also shown in this figure. Figure 10 also compares

the results of the deterministic and stochastic models for varied numbers of initially existing individuals in the basin of attraction of the equilibrium point E_{4^*} to show how demographic stochasticity impacts the persistence of the species in the population. We can see from this figure that the deterministic model consistently displays the persistence of both prey species, while the stochastic model consistently displays only the extinction of the second prey species from the population. In subsection 4.2, we derive an implicit equation for the expected time to population extinction since there is a possibility of population extinction in a finite amount of time. After deriving the implicit equation for the expected time to population extinction, in Figure 11, we graphically present the effect of the carrying capacities on the extinction time. From this figure, it is clear that the carrying capacity of patch 1 has a greater impact on extinction time than the carrying capacity of patch 2 (see Figure 11).

Data availability

No data was used for the research described in the article.

Acknowledgements

Debjani Mondal's research is supported by University Grant Commission, India (Student Id:191620134263).

Conflict of interest

Not Applicable.

Appendix A: Gillespie algorithm [9]

The basic idea of our considered Gillespie algorithm is to use Monte Carlo technique to simulate the stochastic process. Suppose we have a system of

M-state transitions. Let $q_i(t)$ represent the propensity function of the ith transition, where i ranges from 1 to M, at a given time t. This means that $q_i(t)\ dt$ represents the probability of the ith transition occurring within the time interval $[t, t + dt)$. Table 4 provides the propensity functions (transition rates) for our developed stochastic model. Then the Gillespie algorithm consists of the following steps at time t:

(i) Set the initial condition(s) for each state at $t = 0$.

(ii) Generate two random numbers r_1 and r_2 uniformly distributed in $(0, 1)$.

(iii) Compute the propensity function $q_i(t)$ of each reaction. Compute

$$q = \sum_{i=1}^{M} q_i(t).$$

(iv) Compute the time when the next transition takes place as $t + \tau$, where

$$\tau = \frac{1}{q} \ln\left(\frac{1}{r_1}\right).$$

(v) Compute which reaction occurs at time $t + \tau$. Find j such that

$$r_2 \geq \frac{1}{q} \sum_{i=1}^{j-1} q_i(t) \quad \text{and} \quad r_2 < \frac{1}{q} \sum_{i=1}^{j} q_i(t).$$

Then the jth transition takes place, so update the number of individuals of species corresponding to the occurred state transition.

(vi) Iterate Step (ii) through Step (v) until $t \geq t_{stop}$.

The description of the above simulation algorithm is complete. There are various procedures, such as the direct method and the first-reaction method, to generate the interevent time $t1$ and determine which transition occurs in time $t + t1$. Both of these methods are rigorous and exact, but if the number of state transitions M exceeds 3, then the direct method should be a bit more efficient. In this investigation, the number of state transitions is more than 3. As a result, we have used the direct method to obtain a more efficient result. Furthermore, we cannot solve the forward Kolmogorov differential equation analytically for the CTMC model; hence, we can simulate the stochastic model and produce its sample paths using this technique.

References

[1] Akhi, A.A., Kamrujjaman, M., Nipa, K.F., and Khan, T. *A continuous-time Markov chain and stochastic differential equations approach for modeling malaria propagation*, Healthcare Analytics 4 (2023), 100239.

[2] Allen, L.J. An introduction to stochastic processes with applications to biology, CRC press, 2010.

[3] Allen, L.J. *A primer on stochastic epidemic models: Formulation, numerical simulation, and analysis*, Infect. Dis. Model. 2 (2) (2017), 128–142.

[4] Allen, L.J., and Lahodny Jr, G.E. *Extinction thresholds in deterministic and stochastic epidemic models*, J. Biol. Dyn. 6 (2) (2012), 590–611.

[5] Allen, L.J., and vanden Driessche, P. *Relations between deterministic and stochastic thresholds for disease extinction in continuous-and discrete-time infectious disease models*, Math. Biosci. 243, 1 (2013), 99–108.

[6] Bhowmick, A.R., Bandyopadhyay, S., Rana, S., and Bhattacharya, S. *A simple approximation of moments of the quasi-equilibrium distribution of an extended stochastic theta-logistic model with non-integer powers*, Math. Biosci. 271 (2016), 96–112.

[7] Crépin, A.-S., Biggs, R., Polasky, S., Troell, M., and DeZeeuw, A. *Regime shifts and management*, Ecol. Econ. 84 (2012), 15–22.

[8] Ditlevsen, S., and Samson, A. *Introduction to stochastic models in biology*, Stochastic Biomathematical Models: With Applications to Neuronal Modeling, (2013) 3–35.

[9] Gillespie, D.T. *A general method for numerically simulating the stochastic time evolution of coupled chemical reactions*, J. Comput. Phys. 22 (4) (1976), 403–434.

[10] Hale, J.K. *Functional differential equations*, In Analytic Theory of Differential Equations: The Proceedings of the Conference at Western

Michigan University, Kalamazoo, from 30 April to 2 May 1970 (2006), Springer, 9–22.

[11] Hilker, F.M., Langlais, M., and Malchow, H. *The Allee effect and infectious diseases: extinction, multistability, and the (dis-) appearance of oscillations*, Am. Nat. 173 (1) (2009), 72–88.

[12] Jang, S. R.-J., and Baglama, J. *Continuous-time predator–prey models with parasites*, J. Biol. Dyn. 3 (1) (2009), 87–98.

[13] Maity, S., and Mandal, P.S. *A comparison of deterministic and stochastic plant-vector-virus models based on probability of disease extinction and outbreak*, Bull. Math. Biol. 84 (3) (2022), 41.

[14] Maity, S., and Mandal, P.S. *The effect of demographic stochasticity on Zika virus transmission dynamics: Probability of disease extinction, sensitivity analysis, and mean first passage time*, Chaos: An Interdisciplinary Journal of Nonlinear Science 34 (3) (2024).

[15] Maliyoni, M. *Probability of disease extinction or outbreak in a stochastic epidemic model for west Nile virus dynamics in birds*, Acta Biotheor. 69 (2) (2021), 91–116.

[16] Maliyoni, M., Chirove, F., Gaff, H.D., and Govinder, K.S. *A stochastic tick-borne disease model: Exploring the probability of pathogen persistence*, Bull. Math. Biol. 79 (2017), 1999–2021.

[17] Maliyoni, M., Chirove, F., Gaff, H.D., and Govinder, K.S. *A stochastic epidemic model for the dynamics of two pathogens in a single tick population*, Theor. Popul. Biol. 127 (2019), 75–90.

[18] Mandal, P.S., Allen, L.J., and Banerjee, M. *Stochastic modeling of phytoplankton allelopathy*, Appl. Math. Model. 38, (5-6) (2014), 1583–1596.

[19] Mandal, P.S., Kumar, U., Garain, K., and Sharma, R. *Allee effect can simplify the dynamics of a prey-predator model*, J. Appl. Math. Comput. 63 (2020), 739–770.

[20] Mandal, P.S., and Maity, S. *Impact of demographic variability on the disease dynamics for honeybee model*, Chaos: An Interdisciplinary Journal of Nonlinear Science 32 (8) (2022), 083120.

[21] Nandi, A., and Allen, L.J. *Stochastic multigroup epidemic models: Duration and final size*, Modeling, Stochastic Control, Optimization, and Applications (2019), 483–507.

[22] Ndii, M.Z., and Supriatna, A.K. *Stochastic mathematical models in epidemiology*, Information 20 (2017), 6185–6196.

[23] Nipa, K.F., Jang, S. R.-J., and Allen, L.J. *The effect of demographic and environmental variability on disease outbreak for a dengue model with a seasonally varying vector population*, Math. Biosci. 331 (2021), 108516.

[24] Perko, L. Differential equations and dynamical systems, vol.7. Springer Science & Business Media, 2013.

[25] Polovina, J.J. *Climate variation, regime shifts, and implications for sustainable fisheries*, Bull. Marine Sci.76 (2) (2005), 233–244.

[26] Saha, B., Bhowmick, A.R., Chattopadhyay, J., and Bhattacharya, S. *On the evidence of an Allee effect in herring populations and consequences for population survival: A model-based study*, Ecol. Model. 250 (2013), 72–80.

[27] Sau, A., Bhattacharya, S., and Saha, B. *Recognizing and prevention of probable regime shift in density regulated and Allee type stochastic harvesting model with application to herring conservation*, arXiv preprint arXiv:2108.07534 (2021).

[28] Sau, A., Saha, B., and Bhattacharya, S. *An extended stochastic Allee model with harvesting and the risk of extinction of the herring population*, J. Theor. Biol. 503 (2020), 110375.

[29] Scheffer, M., Carpenter, S., Foley, J.A., Folke, C., and Walker, B. *Catastrophic shifts in ecosystems*, Nature 413, 6856 (2001), 591–596.

[30] Scheffer, M., and Carpenter, S.R. *Catastrophic regime shifts in ecosystems: linking theory to observation*, Trend Ecol. Evol. 18 (12) (2003), 648–656.

[31] Sen, M., and Banerjee, M. *Rich global dynamics in a prey–predator model with Allee effect and density dependent death rate of predator*, Inter. J. Bifurcat.Chaos 25, 03 (2015), 1530007.

[32] Sibly, R.M., Barker, D., Denham, M.C., Hone, J., and Pagel, M. *On the regulation of populations of mammals, birds, fish, and insects*, Science 309 (5734) (2005), 607–610.

[33] Stephano, M.A., Irunde, J.I., Mwasunda, J.A., and Chacha, C.S. *A continuous time Markov chain model for the dynamics of bovine tuberculosis in humans and cattle*, Ricerche di Matematica (2022), 1–27.

[34] Swift, R.J. *A stochastic predator-prey model*, Irish Math. Soc. Bull. 48, 57-63 (2002), 646.

[35] Vishwakarma, K., and Sen, M. *Role of Allee effect in prey and hunting cooperation in a generalist predator*, Math. Comput. Simul. 190 (2021), 622–640.